

Circular polarization signals of cloudy (exo)planets

L. Rossi and D. M. Stam

Faculty of Aerospace Engineering, Delft University of Technology, Kluyverweg 1, 2629 HS Delft, The Netherlands

Received XX, 2018; accepted YY, 2018

ABSTRACT

Context. The circular polarization of light that planets reflect is often neglected because it is very small compared to the linear polarization. It could, however, provide information on a planet's atmosphere and surface, and on the presence of life, because homochiral molecules that are the building blocks of life on Earth are known to reflect circularly polarized light.

Aims. We compute P_c , the degree of circular polarization, of light that is reflected by rocky (exo)planets to provide insight into the viability of circular spectropolarimetry for characterizing (exo)planetary atmospheres.

Methods. We compute the P_c of light that is reflected by rocky (exo)planets with liquid water or sulfuric acid solution clouds, both spatially resolved across the planetary disk and, for planets with patchy clouds, integrated across the planetary disk, for various planetary phase angles α .

Results. The optical thickness and vertical distribution of the atmospheric gas and clouds, the size parameter and refractive index of the cloud particles, and α all influence P_c . Spatially resolved, P_c varies between $\pm 0.20\%$ (the sign indicates the polarization direction). Only for small gas optical thicknesses above the clouds do significant sign changes (related to cloud particle properties) across the planets' hemispheres occur. For patchy clouds, the disk-integrated P_c is typically smaller than $\pm 0.025\%$, with maximums for α between 40° and 70° , and 120° to 140° . As expected, the disk-integrated P_c is virtually zero at $\alpha = 0^\circ$ and 180° . The disk-integrated P_c is also very small at $\alpha \approx 100^\circ$.

Conclusions. Measuring circular polarization signals appears to be challenging with current technology. The small atmospheric circular polarization signal could, however, allow the detection of circular polarization due to homochiral molecules such as those associated with life on Earth. Confirmation of the detectability of such signals requires better knowledge of the strength of circular polarization signals of biological sources and in particular of the angular distribution of their scattering.

Key words. Polarization – Techniques: polarimetric – Radiative transfer – Planets and satellites: atmospheres

1. Introduction

Polarimetry has been shown to be a strong tool for the characterization of solar system planets, with the successful characterization of the clouds of Venus (Hansen & Hovenier 1974), the studies of atmospheres of other planets such as those of Jupiter (see e.g. McLean et al. 2017, and references therein), Saturn (Tomasko & Doose 1984), Uranus, and Neptune (Schmid et al. 2006), and airless bodies such as comets and asteroids (Kiselev et al. 2015; Cellino et al. 2015, and references therein). There is also a great potential for polarimetry of exoplanets because the light emitted by solar-type stars can be assumed to be unpolarized when integrated across their disk (Kemp et al. 1987), while it is usually polarized upon reflection by a planet. Polarimetry can thus increase the contrast between background starlight and a planet (Seager et al. 2000; Lucas et al. 2009), and ease the detection and confirmation of an exoplanet. And, because the degree and direction of polarization are sensitive to the composition and structure of a planetary atmosphere and surface, polarimetry could also help to characterize an exoplanet (see e.g. Seager et al. 2000; Karalidi et al. 2012; Stam et al. 2004; Stam 2008).

Like the state of linear polarization, the state (degree and direction) of circular polarization can contain information about the structure and composition of a planetary atmosphere and about the properties of a planetary surface. Circular polarization is typically induced through the multiple scattering of light by

non-gaseous, atmospheric particles (Hansen & Hovenier 1974), or through the multiple reflection of light by a rough surface (Kemp & Wolstencroft 1971), but, interestingly, it also displays potential for use in the detection of life (MacDermott et al. 1996; Bailey 2000; Sparks et al. 2005). This is due to the preferred orientation of the chiral molecules that make up organisms on Earth, referred to as homochirality (Bonner 1991), which induces distinctive circular polarization variations with wavelengths in reflected and transmitted light (Nagdimunov et al. 2013; Sparks et al. 2012, 2009; Patty et al. 2017), although measurements on two types of cyanobacteria species by Martin et al. (2016) also suggest that measured circular polarization signals can be due to internal reflections and thus not necessarily due to homochirality.

While many studies have concentrated on the state of the linear polarization of light, few have considered circular polarization of reflected sunlight. Indeed, only a handful of measurements of the state of circular polarization of solar system planets are available (Kemp & Wolstencroft 1971; Swedlund et al. 1972; Wolstencroft 1976; Kawata 1978; Sparks et al. 2012; Meierhenrich et al. 2002), all obtained with Earth-based telescopes. As far as we know, there has not been a space-based instrument with circular polarization measurement capabilities targeting planets. Measuring the circular polarization requires more complicated instrumentation (often with more, and moving, parts) than measuring the linear polarization (Sparks et al. 2012), also because the degree of circular polarization is usually very small, especially when compared to the degree of linear polarization. The

Send offprint requests to: D. M. Stam e-mail: d.m.stam@tudelft.nl

instrument requirements for circular polarization instruments, in particular the limits on the cross-talk, are thus very high. Recent advances in the design and production of optical elements, however, are increasing the viability of circular polarimetry as a tool for planetary characterization. In addition, the possibility of detecting circular polarization of light reflected by chiral molecules and thus possibly of detecting life, has increased the interest in circular polarization signals of (exo)planets.

Therefore, this study acts as a starting point for an investigation into the feasibility of the use of circular polarimetry for planetary observations and the identification of homochirality. Circular polarization can be induced by a planetary atmosphere, surface, or a biological presence and it is important to understand the influence that these processes have on the total circular polarization profile of the planet. However, the degree of circular polarization coming from the surface of the planet is irrelevant if it is not visible due to an overwhelming signal from the atmosphere. Therefore, it is vital that the influence of the atmospheric properties on the circular polarization signal of an exoplanet is first studied.

In this paper we investigate the effects of clouds on the degree and direction of circular polarization of light reflected by Earth-like planets for both spatially resolved and disk-integrated measurements. The latter would be representative for (future) measurements of starlight reflected by Earth-like exoplanets. In Sect. 2, we describe the numerical algorithm to compute the polarization signals and provide the physical properties of the atmospheres, including the clouds, and the surfaces that cover our model planets. In Sect. 3, we present calculated polarization signals for planets with different cloud optical thicknesses, micro-physical cloud properties, cloud top altitude, and fractional cloud coverage. In Sect. 4 we discuss the limits of our simulations and the possible issues that observers might face. Finally, in Sect. 5, we summarize our results.

2. Numerical algorithms

2.1. Defining fluxes and polarization

We describe the starlight that is incident on a planet and the starlight that is reflected by the planet by a Stokes vector \mathbf{F} , as (see e.g. Hansen & Travis 1974; Hovenier et al. 2004)

$$\mathbf{F} = \begin{bmatrix} F \\ Q \\ U \\ V \end{bmatrix}, \quad (1)$$

where F describes the total flux, Q and U the linearly polarized fluxes, and V the circularly polarized flux. We express these fluxes in W m^{-2} . Linearly polarized fluxes Q and U are defined with respect to a reference plane, for which we use the planetary scattering plane, that is, the plane that contains (the centre of) the star, the planet, and the observer. Parameters Q and U can straightforwardly be redefined with respect to another reference plane, such as the optical plane of an instrument, using a so-called rotation matrix (see Hovenier & van der Mee 1983, for the definition).

The circularly polarized flux V is 'the excess of flux transmitted by an instrument that passes right-handed circular polarization, over that transmitted by an instrument that passes left-handed circular polarization' (Hansen & Travis 1974). Regarding starlight that is reflected by a planet and that arrives at an observer, parameter V will thus be positive if the observer 'sees' the electric vector rotating in the anticlockwise direction, and V

will be negative if the observer 'sees' a rotation in the clockwise direction.

We assume that the starlight that is incident on a planet is unidirectional and unpolarized. The justification of the latter is based on the very small values of the disk-integrated polarization of solar-type stars. Kemp et al. (1987) give measurements of the linear and circular polarization of the Sun: their disk-integrated measurements yield maximal values of 0.8×10^{-6} for the linear polarization, and -1×10^{-6} for the circular polarization, with a B filter. Locally, disturbances on the stellar disk such as stellar spots or transiting planets could produce a break in the symmetry of the stellar disk and generate non-zero disk-integrated values of polarization. The values expected from such disturbances are on the order of 10^{-6} for the degree of linear polarization (Berdyugina et al. 2011; Kostogryz et al. 2015). The incident light is thus described as $\mathbf{F}_0 = F_0 \mathbf{1}$, with πF_0 the stellar flux measured perpendicular to the direction of propagation, and $\mathbf{1}$ the unit column vector.

Starlight that is reflected by an orbiting planet will usually be polarized because it has been scattered by gases and aerosols or cloud particles in the planetary atmosphere and/or has been reflected by the surface. The degree of polarization of the reflected starlight is defined as

$$P = \frac{\sqrt{Q^2 + U^2 + V^2}}{F}, \quad (2)$$

the degree of linear polarization as

$$P_1 = \frac{\sqrt{Q^2 + U^2}}{F}, \quad (3)$$

and the degree of circular polarization as

$$P_c = \frac{V}{F}. \quad (4)$$

Following the description above, if $P_c > 0$, the observer 'sees' the electric vector of the light rotating in the anticlockwise direction, and if $P_c < 0$, the observer 'sees' a rotation in the clockwise direction.

2.2. The radiative transfer algorithm

In this paper, we will present computed (polarized) fluxes and polarization for both *spatially resolved* and *spatially unresolved* planets. The latter, for which we integrate the spatially resolved signals across the planetary disks, apply to (future) observations of exoplanets, while the former apply to observations of solar system planets and also helps us to understand the computed exoplanet signals.

For our spatially resolved computations, we first divide the two-dimensional (2D) planetary disk facing the observer into equal-sized, square pixels, with 30 or 100 pixels along the equator of the disk, which is assumed to run horizontally through the middle of the disk. Then, we project the centre of each pixel onto the three-dimensional (3D) planet and determine the following angles for each projected pixel centre on the planet: θ_0 , the angle between the local vertical and the direction towards the illuminating sun or star, θ , the angle between the local vertical and the direction towards the observer, and the azimuthal difference angle $\phi - \phi_0$, which is the angle between the plane containing the local vertical and the propagation direction of the incident light and the plane containing the local vertical and the direction towards the observer (for a detailed definition, see de Haan et al.

1987). The angles depend on the latitude and longitude of the projected pixel centre, and θ_0 and ϕ_0 also depend on the planet's phase angle α , that is, the angle between the star and the observer as measured from the centre of the planet ($0^\circ \leq \alpha \leq 180^\circ$).

Next, we calculate for each pixel, the Stokes vector (see Eq. 1) of the starlight that is reflected at the projected pixel centre on the planet, using

$$\mathbf{F}(\theta, \theta_0, \phi - \phi_0) = \cos \theta_0 \mathbf{R}_1(\theta, \theta_0, \phi - \phi_0) \mathbf{F}_0, \quad (5)$$

with \mathbf{R}_1 the first column of the 4×4 local planetary reflection matrix. Only the first column is relevant, since the incoming starlight is assumed to be unpolarized. The actual area on the planet that is covered by a projected pixel varies with latitude and longitude on the planet, but because all pixels have the same size, their respective Stokes vectors as computed according to Eq. 5 contribute equally to the planetary signal. With our pixels covering the planetary disk, we can straightforwardly model horizontally inhomogeneous planets by choosing different atmosphere and/or surface models for different pixels. The physical properties of our models are described in Sect. 2.3.

Given an atmosphere–surface model for a given pixel, we use an adding–doubling algorithm that fully includes polarization for all orders of scattering (de Haan et al. 1987) to compute the local planetary reflection matrix (see Eq. 5). Rather than embarking on a separate radiative transfer computation for every pixel, we choose to first compute and store the coefficients $\mathbf{R}_1^m(\theta, \theta_0)$ ($0 \leq m < M$, with M the total number of coefficients) of the expansion of $\mathbf{R}_1(\theta, \theta_0, \phi - \phi_0)$ into a Fourier series (see de Haan et al. 1987, for the description of this expansion for the reflection matrix) for the different atmosphere–surface models that occur on our model planet. Our adding–doubling algorithm computes these coefficients at values of $\cos \theta_0$ and $\cos \theta$ that coincide with Gaussian abscissae (the total number of which is user–defined), and additionally for $\theta_0 = 0^\circ$ and $\theta = 0^\circ$. Given a pixel with its local angles θ_0 , θ , and $\phi - \phi_0$, we can efficiently compute its \mathbf{R}_1 by summing up (see de Haan et al. 1987) the Fourier coefficients stored for the relevant atmosphere–surface model, interpolating for values of θ_0 and θ when necessary.

Each pixel is independent from its neighbours; there is no 3D cross–pixel propagation of light. This remains a good approximation considering that the projected area of each pixel on the planet is quite large, meaning that the cross–pixel propagation will occur on scales quite small compared to the pixel size. Furthermore, the case most likely to be affected is that of an inhomogeneous cloud cover (in particular at the edge of clouds). But in our simulations of inhomogeneous covers (see Sect. 3.2), we consider averages over 300 cloud realisations, which we expect should make the effect of horizontal propagation of light negligible.

To compute the disk–integrated Stokes vector, we sum up the Stokes vectors pertaining to the pixels covering the planetary disk. A locally reflected Stokes vector as computed by our adding–doubling algorithm is defined with respect to the local meridian plane, which contains both the local vertical direction and the direction towards the observer. This is perfectly fine when our aim is to compare degrees of polarization between different pixels, because degrees of polarization are independent of the reference plane. However, for every pixel we redefine the local vector to the common reference plane (the planetary scattering plane) using the so-called rotation matrix \mathbf{L} and β , the angle between the local meridian plane and the planetary scattering plane (see Hovenier & van der Mee 1983). This is done before summing up local Stokes vectors for the disk–integration.

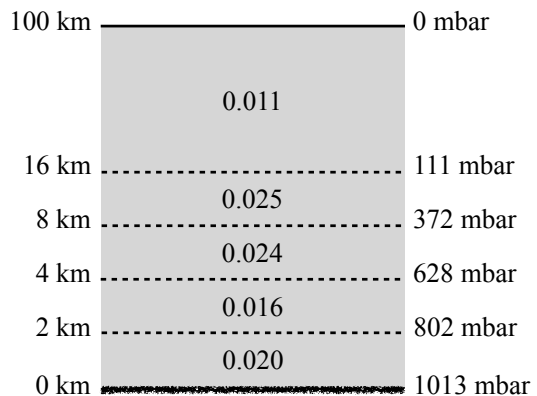


Fig. 1: Gaseous optical thickness b_m at 550 nm in layers comprising the model atmosphere. The altitude and pressure of the levels bounding the layers are also given. The total gaseous optical thickness of the model atmosphere is 0.096.

We normalize disk–integrated flux vectors such that the reflected flux at $\alpha = 0^\circ$ equals the planet's geometric albedo (see Stam et al. 2004; Stam 2008). The degrees of total, linear, and circular polarization, P , P_l , and P_c , are relative measures (see Eqs. 2 – 4) and thus independent of a normalization. The degrees of polarization computed in this paper pertain only to the planet. The polarization of the system as a whole would be lower as the star would add mostly unpolarized flux. We ignore sources of noise such as zodiacal or interstellar dust, or instrumental polarization.

2.3. The model atmospheres and surfaces

The atmosphere and surface of our model planets are assumed to be locally horizontally homogeneous and flat. Unless stated otherwise, the surface below the atmosphere is Lambertian, that is, an isotropic and completely depolarizing surface. Its albedo is indicated by A_s . In this paper, we use $A_s = 0.0$ for the whole planetary surface, unless specified otherwise.

The atmosphere can be vertically inhomogeneous: it is composed of a stack of homogeneous layers. Each layer contains gaseous molecules that are anisotropic Rayleigh scatterers with a depolarization factor of 0.0279 (see Hansen & Travis 1974), and, optionally, cloud particles. The amount of gas and cloud particles in a layer is represented by the optical thicknesses b_m and b_c , respectively. The total gaseous optical thickness of our model atmosphere (thus summed over all layers) is 0.096, which is representative for the Earth's atmosphere at a wavelength of about 550 nm (see Stam 2008, for a detailed description of how b_m is computed). We ignore absorption by atmospheric gases. Figure 1 shows how this optical thickness is divided over five atmospheric layers. The cloud particles are distributed homogeneously within one of these layers.

The single scattering matrix of most types of atmospheric scatterers is given by (see Hansen & Travis 1974)

$$\mathbf{P}(\Theta) = \begin{bmatrix} P_{11}(\Theta) & P_{21}(\Theta) & 0 & 0 \\ P_{21}(\Theta) & P_{22}(\Theta) & 0 & 0 \\ 0 & 0 & P_{33}(\Theta) & -P_{34}(\Theta) \\ 0 & 0 & P_{34}(\Theta) & P_{44}(\Theta) \end{bmatrix}, \quad (6)$$

with Θ the single scattering angle ($0^\circ \leq \Theta \leq 180^\circ$, with $\Theta = 0^\circ$ indicating forward scattered light).

For (anisotropic) Rayleigh scattering, matrix element P_{34} equals zero. Consequently, if Rayleigh scattering is the only scattering process in a planetary atmosphere, incident unpolarized light cannot become circularly polarized by scattering in the atmosphere, not even when it is scattered multiple times. For atmospheric particles that are large compared to the wavelength of the incident light, such as cloud particles, element P_{34} is non-zero for most values of Θ . Unpolarized incident light can thus become circularly polarized when it is scattered at least twice by such particles (or first at least once by a Rayleigh scatterer and then by a large aerosol or cloud particle).

We assume that the particles constituting the clouds are spherical and internally homogeneous. We compute their single scattering matrix with the Mie-scattering algorithm described by de Rooij & van der Stap (1984). The sizes of the cloud particles follow the two-parameter gamma distribution, with an effective radius r_{eff} and an effective variance v_{eff} . Our standard values for r_{eff} and v_{eff} are $8.0 \mu\text{m}$ and 0.1 , respectively, similar to Earth cloud values from Han et al. (1994). For the refractive index we use $1.33 + 10^{-8}i$, which is representative for liquid water at 550 nm (Hale & Querry 1973). The single scattering albedo of these particles is close to one. We will also use Venus-like cloud particles, described by the same size distribution, except with $r_{\text{eff}} = 1.05 \mu\text{m}$, $v_{\text{eff}} = 0.07$, and with a refractive index of $1.44 + 0.015i$, which is representative for a sulfuric acid solution at 500 nm (Hansen & Hovenier 1974). The single scattering albedo of the Venus-like particles is 0.75 .

Figure 2 shows the elements of the scattering matrix for the two types of cloud particles. As can be seen from Eqs. 3 and 6, the ratio P_{21}/P_{11} describes the degree of linear polarization of incident unpolarized light that has been scattered only once. In Fig. 2, we have included a minus sign for this ratio to indicate the direction of polarization of the scattered light: if $-P_{21}/P_{11} > 0$, the scattered light is polarized perpendicular to the plane that contains both the incoming and the scattered beams, while if $-P_{21}/P_{11} < 0$, it is polarized parallel to this plane.

The curves in Fig. 2 clearly show the strong forward scattering peak in the phase functions (elements P_{11}) of both cloud particle types, and the enhanced scattering representative for the first and second order rainbows, around $\Theta = 140^\circ$ and 125° , respectively, in the phase function of the water cloud particles. These rainbow features also show up in other matrix elements, in particular in $-P_{21}/P_{11}$.

2.4. The cloud cover

To investigate the sensitivity of the circularly polarized flux due to the cloud optical thickness, cloud particle properties (size and composition), and cloud top altitude, we will show fluxes and degrees of polarization calculated for planets that are completely covered by a cloud deck. The disk-integrated circularly polarized flux (and degree of circular polarization) of a horizontally homogeneous planet will be zero, because the circularly polarized flux of a pixel on the northern hemisphere will be cancelled

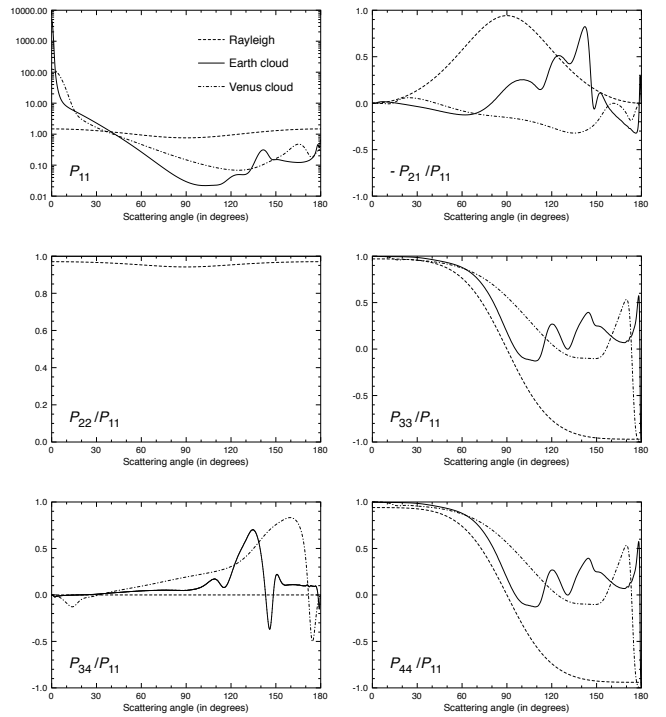


Fig. 2: Single scattering matrix elements of Earth-like cloud particles (solid lines), Venus-like cloud particles (dashed-dotted lines), and Rayleigh scattering molecules (dashed lines) at $0.55 \mu\text{m}$. Elements P_{11} have been normalized such that their averages over all scattering angles equal one, and the other elements have been normalized to P_{11} . For spherical particles, such as the cloud particles, $P_{22}/P_{11} = 1$, $P_{34} = -P_{43}$, and $P_{33} = P_{44}$. The Earth-like cloud particles are described by a two-parameter gamma size distribution with $r_{\text{eff}} = 8.0 \mu\text{m}$ and $v_{\text{eff}} = 0.1$. Their refractive index is $1.33 + 10^{-8}i$ (Hale & Querry 1973). The Venus-like cloud particles have $r_{\text{eff}} = 1.05 \mu\text{m}$, $v_{\text{eff}} = 0.07$, and a refractive index of $1.44 + 0.015i$ (Hansen & Hovenier 1974).

by that of the corresponding pixel on the southern hemisphere, as that would have the same absolute value but the opposite sign (this can be seen in Fig. 3). Thus, to simulate the circularly polarized fluxes of spatially unresolved planets, such as exoplanets, we will use horizontally inhomogeneous model planets that are asymmetric with respect to the planetary scattering plane due to patchy clouds. We will limit ourselves to a single type of cloud per planet, thus, the clouds in all cloudy pixels have the same optical thickness, altitude, and particle properties.

The patchy clouds are described by f_c , the fraction of all pixels on the whole disk that are cloudy, and by the actual distribution of the cloudy pixels across the disk. The patches are generated with the method described by Rossi & Stam (2017), where cloudy pixels are defined by a 2D Gaussian, randomly placed on the square grid and which shape and orientation are chosen to simulate streaky, zonally-oriented, clouds. Figure 5 shows examples of cloud patterns for $f_c = 0.3$ (i.e. 30 % cloud cover) and $f_c = 0.5$.

For each cloud cover pattern across a planet, we define the asymmetry factor γ , which indicates the percentage of pixels (cloudy and non-cloudy) on one of the illuminated and visible hemispheres that *do not have* a similar pixel in a mirrored posi-

tion on the other hemisphere (assuming that the planetary scattering plane divides the two hemispheres). If $\gamma = 0.0$, all pixels have a mirror pixel (the circular polarization signal of this planet will equal zero), while if $\gamma = 1.0$, none of the pixels has a mirror pixel. The asymmetry factors for the examples shown in Fig. 5 are 0.24 and 0.52 for the two $f_c = 0.3$ cases, and 0.28 and 0.61 for the two $f_c = 0.5$ cases.

3. Results

In this section, we will first show and discuss the reflected total and polarized fluxes for horizontally homogeneous planets (Sect. 3.1), and then we will investigate the effects of horizontal inhomogeneities due to fractional cloud coverage (Sect. 3.2). For horizontally homogeneous planets, P_c will be zero when integrated across the planetary disk. For these planets, we will therefore only show and discuss signals of spatially resolved planets. Horizontally inhomogeneous planets can have a non-zero disk-integrated value of P_c . The spatially resolved signals of these planets can straightforwardly be derived from the spatially resolved signals of the horizontally homogeneous planets. For the horizontally inhomogeneous planets, we will thus only discuss the spatially unresolved signals, which would be representative for exoplanet observations.

3.1. Horizontally homogeneous planets

As mentioned earlier, a planet with a purely gaseous atmosphere and a depolarizing or linearly polarizing surface will not reflect any circularly polarized flux: circularly polarized flux will only appear when the atmosphere contains aerosol and/or cloud particles. Figure 3 shows the reflected flux F , and the degrees of linear and circular polarization, P_l and P_c , respectively, for a planet at a phase angle $\alpha = 60^\circ$ (the single scattering angle Θ is thus 120° across the planetary disk). The horizontally and vertically homogeneous cloud layer has an optical thickness $b_c = 2.0$ (at 550 nm), its bottom at 2.0 km, and its top at 4.0 km. The clouds are composed of either the Earth-like or the Venus-like particles.

It can be seen that for both particle types, the reflected flux F is fairly constant across the planetary disk, thanks to the homogeneous layer of clouds that hides the dark surface. At the limb, F (per pixel) is largest, because there the reflected light has been mostly scattered by the gas above the cloud, and the scattering phase function of gas molecules is relatively large at this phase angle (i.e. a scattering angle of 120° , see Fig. 2). At the terminator, the incident flux per atmosphere surface area is very small, yielding small values of F .

The degree of linear polarization, P_l , is also fairly constant across the disk, because it is strongly determined by the singly scattered light, and the single scattering angle is constant across the disk. Values of P_l are somewhat higher at the limb and the terminator for both types of cloud particles because there the contribution of multiple scattered light from the lower layers, with usually a low degree of polarization, is relatively small, and there is a stronger contribution of relatively highly polarized light scattered by the molecules higher in the atmosphere. The smallest local values of P_l for the Venus-like cloud particles are smaller than those for the Earth-like cloud particles. That is due to the difference in their single scattering polarization at this phase angle (cf. Fig. 2): indeed, were it not for the gaseous molecules overlying the cloud layer, the Venus-like cloud particles would yield a planet with a polarization direction parallel to the reference plane. Both the gas molecules and the Earth-like cloud

particles yield perpendicular polarization. Integrated across the planetary disks, $P_l = 25.5\%$ for the planet with the Earth-like clouds and 24.5% for the planet with the Venus-like clouds at this phase angle.

The degree of circular polarization, P_c , depends on the multiple scatterings involving a cloud particle at least once. As expected, it is generally small for both types of cloud particles, and the pattern of P_c on the northern hemisphere mirrors that on the southern hemisphere, except with the opposite sign, because of the horizontal homogeneity of the cloud cover. Along the equator, P_c equals zero due to symmetry. Because of this antisymmetry of the circular polarization on the planetary disk, $P_c = 0\%$ for both planets when integrated across the planetary disk.

Through the multiple scattering, P_c depends on the illumination and viewing geometries (hence on the phase angle and the location on the planet) and on the composition and structure of the planetary atmosphere and surface (the latter is black for our model planets). In particular, the gas molecules above the clouds appear to have a significant influence on P_c , because they scatter linearly polarized light onto the clouds, and the cloud particles can subsequently scatter light back to space in a circularly polarized state, through the single scattering matrix element P_{43} (see Fig. 2). Because this element has the same sign for the Earth-like and the Venus-like cloud particles, P_c across the planet has the same sign for both cloud types. The higher value of element P_{43} of the Venus-like particles is responsible for the higher values of P_c across the planet with the Venus-like clouds. Another reason for the difference in the absolute value of P_c is the absorption within the Venus-like cloud particles (their single scattering albedo is 0.75 versus almost 1.0 for the Earth-like particles), which suppresses the multiple scattering of light between cloud particles. Because multiple scatterings between cloud particles randomize and hence usually lower the degree of polarization, less multiple scatterings will usually yield a higher P_c .

The relative importance of the scattering by the gas and the cloud layer on P_c can be analysed more in depth by unravelling the different contributions. Figure B.1 shows P_c for five model atmospheres with varying optical thicknesses of the gas and the cloud, for the two cloud types. The vertical extension of the cloud is from 2.0 and 4.0 km, like in Fig. 3. When filled with gas (models A, B, and C), the optical thickness of the lowest layer is 0.020, otherwise (models D and E) it is zero. The gaseous optical thickness of the second layer is zero (models C and D) or 0.016 (models A, B, and E), and that of the third layer is zero (models B, C, and D) or (cf. Fig. 1) $0.024 + 0.025 + 0.011 = 0.060$ (models A and E). By comparing the signals for the different model atmospheres, it is clear that the gas above the cloud strongly influences P_c : the linearly polarized light scattered downwards by the gas yields circularly polarized light through the single scattering matrix element P_{34} (which equals $-P_{43}$) of the cloud particles for models A and E. Because element P_{34} has the same sign across most of the single scattering angle range for the two cloud particle types (see Fig. 2) and because the incident linearly polarization field of the single scattered light is the same, the sign of P_c is the same for the two types of planets.

For the atmospheres without gas above the cloud (models B, C, and D), P_c shows a pattern that depends on the cloud particle type, as it is mostly due to light that has been scattered twice by the cloud particles. The difference in the P_c pattern is to be expected because the direction of linear polarization of the singly scattered light is different for the different cloud particle types across most of the single scattering angle range, while the direction of circular polarization is the same across the scattering angle range for the different cloud particle types (cf. Fig. 2). In

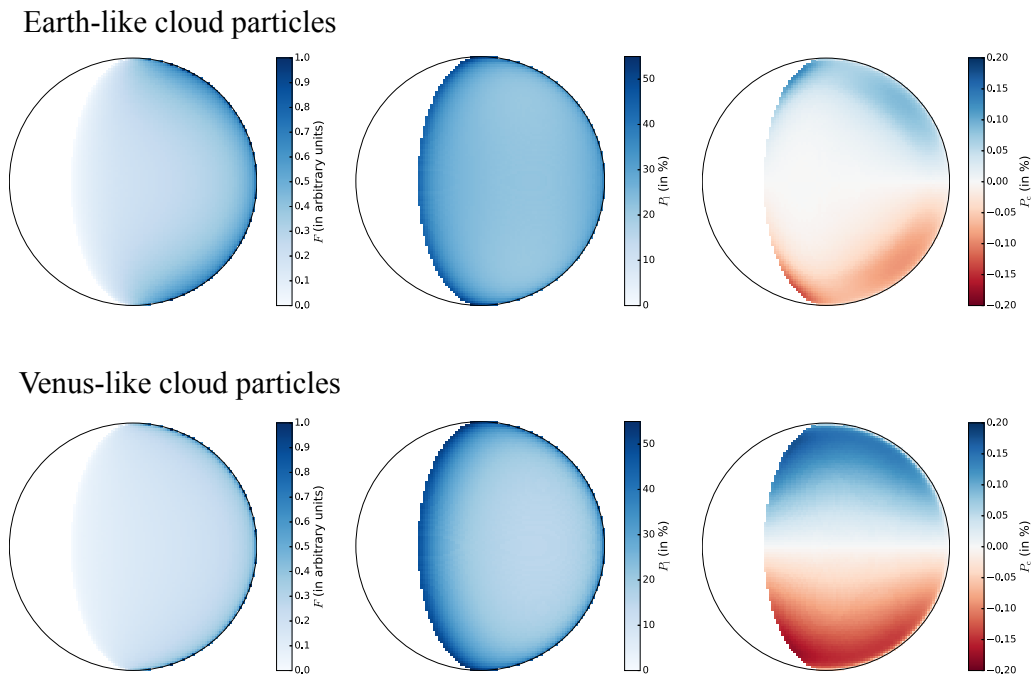


Fig. 3: Reflected light signals of planets with horizontally homogeneous clouds composed of Earth-like cloud particles (top row) or Venus-like cloud particles (bottom row), at a phase angle α of 60° . For each model planet, the cloud optical thickness b_c is 2.0, the cloud bottom is at 2.0 km, its top at 4.0 km (see Fig. 1), and the surface is black. Left column: The total flux F (normalized to the maximum on the disk); middle column: The degree of linear polarization P_1 ; right column: The degree of circular polarization P_c . Integrated across the planetary disk, $P_1 = 25.5\%$ for the Earth-like clouds and 23.8% for the Venus-like clouds, in both cases with the polarization direction perpendicular to the planetary scattering plane.

the absence of (a significant amount of) gas above the clouds, the pattern of P_c across the planet will also depend slightly on the gas within and/or below the clouds. This can be seen by comparing the plots for models B, C, and D in Fig. B.1. This gas within and/or below the clouds can scatter linearly polarized light towards the cloud particles that can subsequently be scattered as circularly polarized light, and the light scattered by the gas can dilute P_c by adding unpolarized light to the signal emerging from the atmosphere.

Next, we investigate the effects of the vertical position of a cloud in a planetary atmosphere (with gas in all atmospheric layers). This position influences P_c because it influences the optical path lengths in the atmosphere, and hence for example the amount of linearly polarized light that is incident on the cloud from above and/or from below. Figure B.2 shows the spatially resolved P_c for the two cloud types with $b_c = 2.0$ with a cloud top altitude z_t equal to 2, 4, 8, 16, and 100 km (see Fig. 1, the cloud fills its atmospheric layer). A cloud top altitude of 100 km, thus at the top of the atmosphere, is unrealistic, but has been included to gain insight in the light scattering processes.

Figure B.2 shows that increasing z_t up to at least $z_t = 8$ km, leads to a decrease of P_c for both cloud types. This decrease is due to the decrease of the linearly polarized, Rayleigh scattered flux that is incident on the top of the cloud. When z_t is increased even further, to 16 and 20 km, the contribution of the gas below the cloud layer to P_c becomes significant. The difference in the amount of gas below the cloud is responsible for the difference in the patterns between the planet plots for model B in Fig. B.1

(a low cloud, hence little gas below the cloud) and those for $\alpha = 60^\circ$ and $z_t = 100$ km in Fig. B.2.

Not only the gas optical thickness influences the optical path through the atmosphere and hence P_c , but also the cloud optical thickness b_c . Figure B.3 shows P_c for Earth-like and Venus-like particles, and for b_c equal to 0.5, 1.0, 2.0, 4.0, and 10.0 at α equal to 30° , 60° , 90° , and 120° . The cloud top in all cases is at 4 km. For the model atmospheres with Earth-like cloud particles, P_c seems largest for $b_c = 2.0$. For smaller b_c , the amount of multiple scattering is too small to induce significant circularly polarized flux, while for increasing b_c above 2.0, the randomizing influence of the increasing multiple scattering decreases V while increasing F , and thus decreases P_c . The latter effect seems smallest at $\alpha = 120^\circ$, because there the optical path lengths for the light reaching the observer are already very long and increasing b_c does not significantly change the contribution of multiple scattered light to the received signal.

The atmospheres with the Venus-like cloud particles show a different behaviour at least for $\alpha = 30^\circ$, 60° , and 90° : P_c increases with increasing b_c until $b_c = 2.0$, and then remains more or less constant. The reason is that the Venus-like cloud particles absorb light, and hence prevent a strong increase in multiple scattered light with increasing b_c and thus prevent a decrease of P_c .

In the results presented so far, the model atmospheres were bounded below by black surfaces. The influence of a reflecting surface on P_c is shown in Fig. 4, where P_c across the planet has been plotted for surface albedo's A_s equal to 0.0 (the stan-

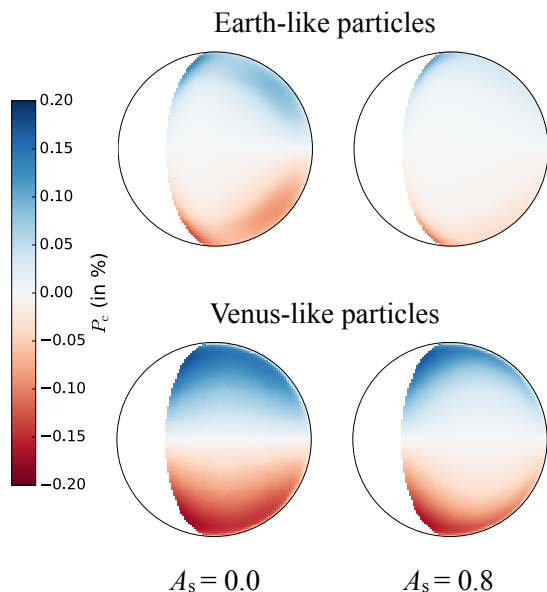


Fig. 4: Degree of circular polarization P_c for the standard model atmosphere with the cloud top at 4 km, b_c equal to 2.0, and Earth-like (top) and Venus-like (bottom) cloud particles. The phase angle is 60° , and the surface albedo A_s equals 0.0 (left column) or 0.8 (right column).

standard model) to 0.8. The surface reflection is Lambertian, that is, isotropic and unpolarized. The atmosphere is the standard model atmosphere (see Fig. 3). The cloud has its top at 4.0 km and $b_c = 2.0$. As expected, increasing A_s adds unpolarized light to the bottom of the cloud layer and decreases P_c . This decrease of P_c with increasing A_s decreases with increasing b_c .

In case the surface below the atmosphere reflects linearly polarized light, it can influence the pattern of P_c across the planet, as this light can be scattered by the cloud particles and become circularly polarized, but the overall effect is expected to be small because in order to have a significant effect, there should be a horizontally homogeneously polarizing surface in combination with a high surface albedo. Even if these surface characteristics were met, a cloudy atmosphere would lead to a relatively low and diffuse surface illumination, limiting the absolute amount of linearly polarized flux that would reach the clouds, especially with larger values of b_c . A circularly polarizing surface, for example covered by vegetation or other organic materials (e.g. Patty et al. 2017; Sparks et al. 2012), could directly contribute to a planet’s circularly polarized flux, thus without requiring an additional scattering by cloud particles. However, if the surface reflection were independent of the azimuthal angle, for example, if the angular distribution of the reflected light were isotropic, the surface would leave no net circular polarization signal at the top of the atmosphere.

3.2. Horizontally inhomogeneous planets

We next investigate the influence of patchy cloud covers and the cloud cover variability on P_c of starlight that is reflected by a spatially unresolved planet, such as an exoplanet. As discussed above, the disk-integrated P_c of a horizontally homo-

geneous planet is zero, as contributions from one hemisphere cancel out those of the other hemisphere. Therefore, only horizontally inhomogeneous planets would yield non-zero values of P_c . As Figs. B.2–4 show, P_c can vary significantly across a horizontally homogeneous cloudy planet, while it is zero in the absence of clouds. So patchy clouds could yield a net amount of circular polarization with P_c depending on the distribution of the patches across the planetary disk. Indeed, even for patchy clouds, any symmetry with respect to the scattering plane will cancel the net circular polarization. A strongly symmetric cloud cover across the planet would yield a relatively low net circular polarization signal, while the most extreme case, a planet with one fully cloudy and one cloud-free hemisphere (asymmetry parameter γ would thus equal 1.0), could yield a relatively large net signal.

We use the cloud algorithm described in Sect. 2.3 (see Rossi & Stam 2017, for a more detailed explanation) to generate 300 different patchy cloud covers for various values of the cloud coverage fraction f_c and compute the disk-integrated degree of circular polarization P_c for planets covered by those cloud patterns at phase angles ranging from 0° to 180° . Examples of cloud patterns are given in Fig. 5.

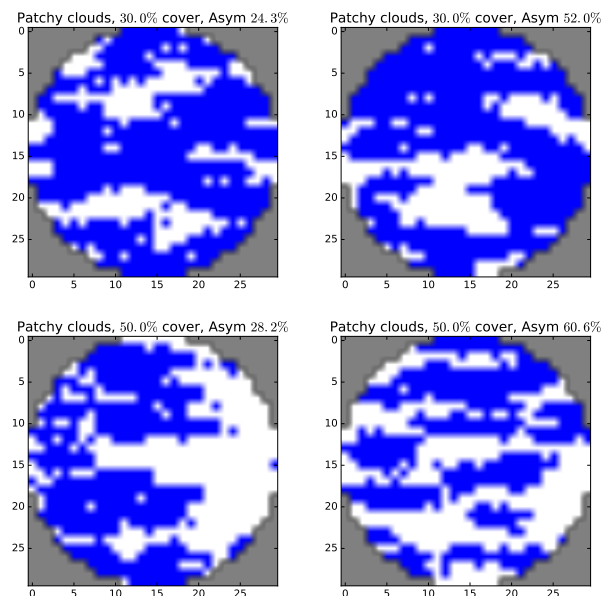


Fig. 5: Examples of patchy cloud patterns for $f_c = 0.3$ (top) and $f_c = 0.5$ (bottom) at $\alpha = 0^\circ$. The asymmetry factors γ of these planets are 0.24 (top-left), 0.52 (top-right), 0.28 (bottom-left) and 0.61 (bottom-right).

Figure 6 shows as functions of α , the maximum and minimum values of P_c as obtained with 300 different cloud patterns for cloud coverage fractions f_c ranging from 0.1 (10% clouds) to 0.9 (90% clouds), for Earth-like and Venus-like cloud particles. The first thing to note are the overall very small values of P_c for these horizontally inhomogeneous planets: the maximum values of P_c are about 0.020% for both the Earth-like, water clouds particles, and the Venus-like, sulfuric acid cloud particles. For both cloud types, these maximum values occur around $\alpha = 50^\circ - 60^\circ$. A second, smaller maximum occurs around $\alpha = 130^\circ$, also for both cloud types. These (local) extreme values of P_c appear to be relatively independent of the cloud fraction f_c ; only for $f_c = 0.1$, the maximum values are slightly smaller.

Measuring P_c thus does not seem to provide insight into the cloud coverage fraction f_c of a planet. This might seem surprising, as on our model planets circularly polarized light is only induced by scattering by the cloud particles. However, it can be explained by looking at the occurrence of cloudy pixels on both sides of the planet’s hemisphere, keeping in mind that the circularly polarized flux of a cloudy pixel on one hemisphere will be ‘cancelled’ if the pixel’s mirror pixel on the other hemisphere is also cloudy. At small cloud coverage fractions, there are few cloudy pixels to contribute circularly polarized flux, while the probability is small that a cloudy pixel has a cloudy mirror pixel on the opposite hemisphere that would cancel its polarized flux contribution. At large cloud coverage fractions, there are many cloudy pixels that contribute circularly polarized flux, but the probability that a cloudy pixel has a cloudy mirror pixel on the opposite hemisphere that cancels its polarized flux contribution is also large.

Apart from the minimum values of P_c at $\alpha = 0^\circ$ and 180° , which are due to geometrical symmetry (note that P_c can deviate slightly from 0.0 at these phase angles due to the horizontal inhomogeneities), P_c shows a clear local minimum around $\alpha = 100^\circ$, with a value of about 0.005% for the Earth-like cloud particles and 0.002% for the Venus-like cloud particles. These local minimum values of the disk-integrated P_c around $\alpha = 100^\circ$ are related to the low spatially resolved values of P_c for $\alpha = 90^\circ$ in Figs. B.2 and B.3. Phase angles close to 90° are usually considered to be the best for direct observations of exoplanets because there the angular distance between a planet and its star will be largest. Our results show that this phase angle range is, however, far from optimal for measurements of the circular polarization of exoplanets. The positive aspect of the low values of P_c in this phase angle range is that the influence of circularly polarized light on measurements of linear polarization, for example through cross-talk between optical elements in an instrument or telescope, will be minimum in this phase angle range. Indeed, this phase angle range is in particular interesting for measurements of the state of the linear polarization of exoplanets with Rayleigh scattering atmospheres, for which P_l will be large (Seager et al. 2000; Stam et al. 2004; Stam 2008).

The small differences in the general shape of the disk-integrated P_c as a function of α of the planets that are covered with water-clouds and those that are covered by sulfuric acid clouds, in particular at small and large phase angles, are indicative of the different light scattering properties of the cloud particles (cf. Fig. 2), but will likely be far too subtle to be useful for cloud particle characterization. Indeed, the state of linear polarization, which has been proven to hold such information (see e.g. Hansen & Hovenier 1974; Hansen & Travis 1974), is expected to be much larger than P_c at most phase angles. The exception being the phase angles where $P_l = 0$ (i.e. the so-called neutral points) but $P_c \neq 0$.

Figure 7 shows the statistics of P_c computed for the 300 cloud patterns as functions of the cloud fraction f_c for $\alpha = 50^\circ$ and 130° , the phase angles where the maximum values of P_c occur in Fig. 6. It can be seen that the distributions are quite symmetrical and have a median quite close to the average value (that is equal to 0.0%), as it should be because the clouds can appear on both hemispheres. As can be seen, the range of values of P_c increases with increasing cloud coverage fraction f_c from 0.1 to 0.4 - 0.5. Then it decreases with increasing f_c , and it is particularly small for $f_c=0.9$, for both phase angles. The very small range in P_c at the largest values of f_c is due to the planetary disk being almost completely cloudy and thus almost symmetric. At $\alpha = 130^\circ$, only a narrow crescent of the planetary disk is illumi-

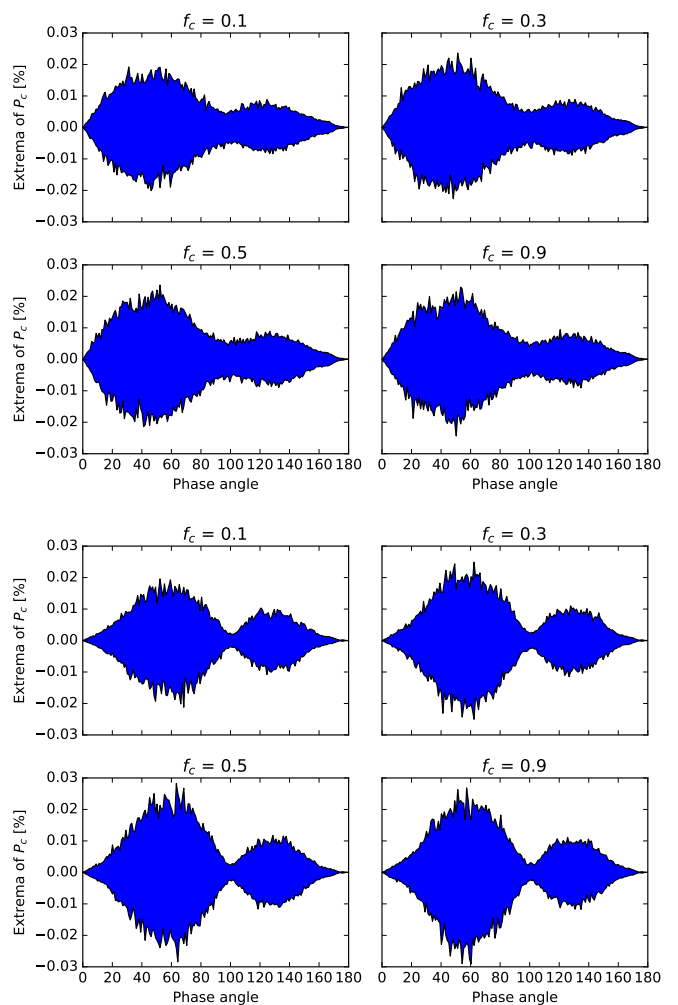


Fig. 6: Maximum values of P_c computed for 300 cloud patterns as a function of phase angle α , for different cloud coverage fractions f_c , and for Earth-like (top) and Venus-like cloud particles (bottom).

nated and visible and the symmetry is even higher, and the range of P_c even smaller, than at $\alpha = 50^\circ$. At $f_c = 0.1$ (10%), on the other hand, the disk is almost devoid of cloudy pixels and the range of P_c is thus small. Like in Fig. 6, the dependence of the range of P_c on f_c at intermediate cloud coverages is small.

4. Discussion

The results of our simulations show that the degree of circular polarization of planets with Earth- or Venus-like cloud particles is really small, especially compared to the linear polarization. We address here some limitations of this study and potential issues that observers trying to measure the circular polarization signals could face.

4.1. Effects of non-Lambertian reflecting surfaces

For a solid planet, the albedo A_s of the surface has a minor influence on the pattern of P_c across a cloudy planet. Increasing A_s generally decreases P_c as the surface reflects isotropically distributed and unpolarized light upwards. Even upon scattering by

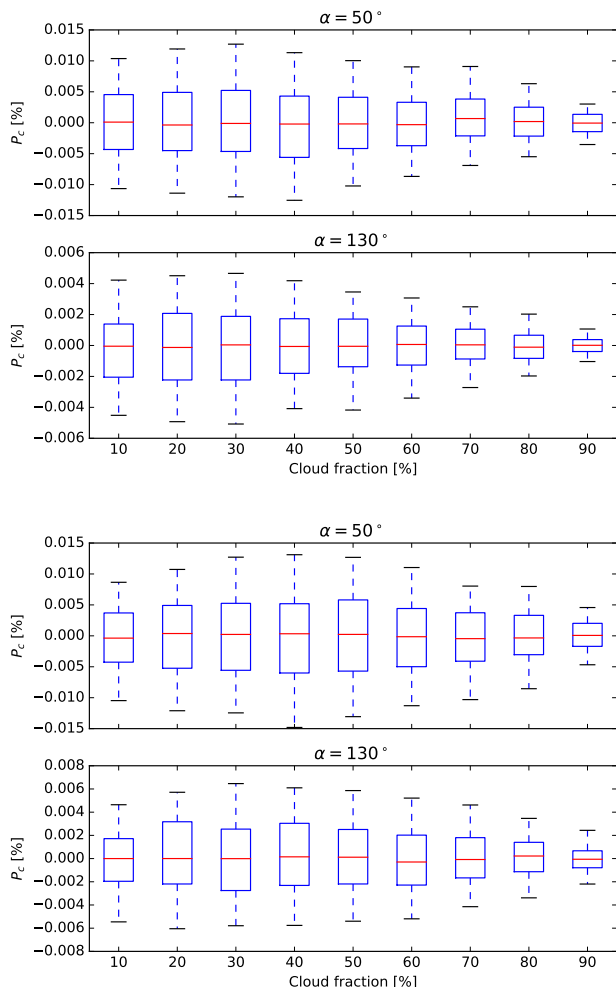


Fig. 7: Box-plots of the distribution of P_c over 300 cloud patterns, for $\alpha = 50^\circ$ and 130° , and the Earth-like (top) and Venus-like (bottom) cloud particles. The box indicates the first and third quartiles, with the median in red. The whiskers show the fifth and 95th percentiles.

the cloud particles, this light will not add any net circularly polarized flux to the pattern of P_c .

A linearly and/or circularly polarizing surface could produce a non-zero planetary P_c , but only if the directional pattern of the linearly and/or circularly polarized flux is azimuthally anisotropic, if the polarizing surface covers a significant part of the planet, and if the diffuse sky flux that is incident on the surface is small compared to the incident direct sunlight or starlight. Due to the lack of azimuthally anisotropically reflecting polarized surface models, the model planets in this paper have Lambertian, that is depolarizing and isotropically reflecting, surfaces.

A thorough investigation of the actual strength of this effect requires a realistic surface reflection model, which is not available now. Circular polarization measurements have been proposed as a technique to search for chiral molecules that on Earth are related to the presence of life (Bailey 2000; Patty et al. 2017; Sparks et al. 2012). Implementing a realistic surface reflection model, possibly based on circular polarization observations of light reflected by (regions on) the Earth or in a laboratory (Patty et al. 2017), thus appears to be a direction worthy of future research.

4.2. Sources of noise

Because we do not include background stellar flux in our computations of the degree of circular polarization, P_c , the exoplanetary signals presented here apply to planets that are spatially resolved from their star. Our results can be adapted for background stellar flux at the location of the planet: if the stellar flux can be considered to be unpolarized it has to be added to the total planetary flux. It will thus lower the observable P_c .

Circular polarization from the interstellar medium or from the zodiacal light could also be a possible source of noise when trying to measure signals from an exoplanet. The zodiacal light is known to present circular polarization, as shown by Wolstencroft & Kemp (1972), with degrees of circular polarization up to -0.8% . We note that the visible-range circular polarization of the zodiacal light varies strongly with the solar longitude and that such measurements have not been reproduced since, leaving our understanding of the circular polarization of the zodiacal light incomplete. The interstellar medium (ISM) also produces polarized light, as non-spherical dust grains can be aligned along lines of magnetic fields, introducing dichroism and birefringence. The amount of circularly polarized light from the ISM shows values on the order of 10^{-4} (Kemp & Wolstencroft 1972; Avery et al. 1975), which is close to our values for disk-integrated signals.

Nevertheless, the spectral dependence of the polarization due to dust in the visible is rather well known (Jones & Whittet 2015). No significant changes are expected to occur on the timescale of observations of an exoplanet, especially when considering that the circular polarization of the planet will vary along the planetary orbit, which could help identify the planetary signal.

4.3. Gaseous absorption

This study ignores the effects of gaseous absorption. The degree of circular polarization in an absorption band could be different from that at continuum wavelengths, because more absorption implies less multiple scattering and a signal originating in higher atmospheric layers. These effects could yield less circular polarization, first because circular polarization arises from multiple scattering but also because higher layers are likely to be pure gas, which does not produce circular polarization. Less multiple scattering would also yield less unpolarized light. So the total degree of circular polarization in an absorption band could also increase with respect to that of the continuum. The change of P_c across an absorption band would thus critically depend on the amount of absorption and on the structure and composition of the atmosphere, just like the change of the degree of linear polarization across absorption bands, as can be seen in for example Fauchez et al. (2017) and Stam et al. (1999). A careful investigation of the behaviour of P_c in the presence of gaseous absorption requires a dedicated study when circular polarization observations in spectral regions with absorption bands are being planned, and is outside the scope of this paper.

5. Summary

We have computed the degree and direction of the circular polarization of planets, both spatially resolved and disk-integrated. The former would be applicable to solar system planets and the latter to exoplanets. Because sunlight or starlight that is incident on a planet is not circularly polarized, purely gaseous atmospheres do not yield any circularly polarized reflected light (cf. the single scattering matrix of Rayleigh scattering in Hansen

& Travis 1974), so all of our planets have cloudy atmospheres. Multiple scattering of incident unpolarized sunlight or starlight by gaseous molecules and then by cloud particles, or between cloud particles, will usually produce a circularly polarized signal.

Spatially resolved simulations of our horizontally homogeneous, cloudy model planets show that P_c is about a factor of 100 smaller than the degree of linear polarization P_l . Furthermore, P_c is mirror symmetric with respect to a planet's light equator (which coincides with the equatorial plane on our planets), except with the opposite sign. On the light equator, P_c is zero.

The pattern of P_c across the planetary disk depends on the type of cloud particles, and on the gaseous scattering optical thickness b_m above, within, and below the clouds, as gas scatters linearly polarized light onto the cloud particles that will subsequently be scattered as (partly) circularly polarized light. For both the water and the sulfuric acid particles comprising our model clouds, a significant amount of gas above the clouds yields positive (negative) P_c across the northern (southern) hemisphere at small phase angles, and negative (positive) P_c across the northern (southern) hemisphere at large phase angles. The sign change appears to happen at phase angles around 90° , except for very small cloud optical thicknesses ($b_c = 0.5$ in Fig. B.3).

Increasing the cloud optical thickness b_c increases the amount of light scattered between the cloud particles, and hence P_c , for b_c up to about 2.0. Increasing b_c even further appears to decrease P_c slightly because then the multiple scattering appears to add mostly to the total flux F . With decreasing b_m above the clouds (i.e. with increasing cloud top altitude and/or increasing wavelength), the pattern of P_c due to the scattering of light between cloud particles becomes dominant. For our model clouds, this pattern shows sign changes and thus regions of zero P_c across each hemisphere.

For horizontally homogeneous planets, the disk-integrated value of P_c is zero, because the circular polarization on the southern hemisphere mirrors that on the northern hemisphere, except with opposite sign. For a horizontally inhomogeneous planet, such as a planet covered by patchy clouds, the disk-integrated P_c is usually not equal to zero. Knowing the values that can be expected for the disk-integrated P_c is important for exoplanetary detections. We therefore investigated the range of values that the disk-integrated P_c might attain for model planets covered by patchy clouds of two different compositions, with different cloud coverage percentages f_c , and different spatial cloud patterns.

For various values of f_c and 300 different cloud patterns, the maximum values of the disk-integrated P_c are about 0.020% for both Earth-like and Venus-like cloud particles. These maximum values occur at phase angles α between about $50^\circ - 60^\circ$. A secondary, smaller maximum occurs around 130° . At $\alpha = 0^\circ$ and 180° , the disk-integrated P_c equals zero due to symmetry (for the horizontally inhomogeneous planet, it can deviate slightly from zero). Another minimum of P_c is smaller than 0.005% and occurs around $\alpha = 100^\circ$, both for the Earth-like and the Venus-like cloud particles. The relative independence of these values to f_c , the cloud pattern, and the cloud particle type implies that measuring P_c of an exoplanet will provide little information on the cloud properties.

In the phase angle range where the disk-integrated P_c is relatively small, around $\alpha = 100^\circ$, P_l , the degree of linear polarization, of a planet with an atmosphere in which gaseous molecules are the main scatterers, will actually be relatively large (Stam et al. 2004; Stam 2008). In this phase angle range, an exoplanet

in a (more or less) circular orbit will have the largest angular distance from its star and thus be a good target for direct measurements of the exoplanet's flux and/or linear polarization signal. Our simulations show that when designing instruments for such measurements, the influence of the circular polarization signal, for example through cross-talk in the optical components, can likely be ignored.

With the aim of this study being to investigate what signals can be observed and their physical origin, we do not explicitly address here the use of circular polarization for characterization of the atmosphere. Measuring the patterns in circular polarization could in principle provide information about the cloud particle properties (size, composition, shape) and atmospheric structure (cloud altitude, thickness). Further research is needed to investigate which information P_c would provide that could not be obtained from flux and in particular linear polarization measurements, as P_l is usually much larger than P_c , and which accuracy would be required for such P_c measurements in order to be able to derive such additional information.

Spatially resolved observations of the visible and infrared circular polarization of the Earth from space would help to validate the radiative transfer codes, our results for the cloudy regions on the planet, and to provide measurements that can be used to develop a realistic circularly polarizing surface model to improve the codes. Such measurements could also be done in a laboratory setting, provided a range of illumination and viewing angles (also including the azimuthal direction) is covered.

Acknowledgements. L. Rossi acknowledges funding through the PEPSci Programme of NWO, the Netherlands Organisation for Scientific Research.

References

- Avery, R. W., Michalsky, J. J., Stokes, R. A., & Ekstrom, P. A. 1975, *AJ*, 80, 1026
- Bailey, J. 2000, in *Astronomical Society of the Pacific Conference Series*, Vol. 213, *Bioastronomy 99*, ed. G. Lemarchand & K. Meech
- Berdyugina, S., Berdyugin, A., Fluri, D., & Pirola, V. 2011, *The Astrophysical Journal Letters*, 728, L6
- Bonner, W. A. 1991, *Origins of Life and Evolution of the Biosphere*, 21, 59
- Cellino, A., Gil-Hutton, R., & Belskaya, I. N. 2015, *Asteroids*, ed. L. Kolokolova, J. Hough, & A.-C. Levasseur-Regourd, 360–378
- de Haan, J. F., Bosma, P. B., & Hovenier, J. W. 1987, *A&A*, 183, 371
- de Rooij, W. A. & van der Stap, C. C. A. H. 1984, *A&A*, 131, 237
- Faucher, T., Rossi, L., & Stam, D. M. 2017, *The Astrophysical Journal*, 842, 41
- Hale, G. M. & Querry, M. R. 1973, *Applied optics*, 12, 555
- Han, Q., Rossow, W. B., & Lacis, A. 1994, *Journal of Climate*, 7, 465
- Hansen, J. E. & Hovenier, J. W. 1974, *Journal of Atmospheric Sciences*, 31, 1137
- Hansen, J. E. & Travis, L. D. 1974, *Space Sci. Rev.*, 16, 527
- Hovenier, J. W., Van Der Mee, C., & Domke, H., eds. 2004, *Astrophysics and Space Science Library*, Vol. 318, *Transfer of polarized light in planetary atmospheres : basic concepts and practical methods*
- Hovenier, J. W. & van der Mee, C. V. M. 1983, *A&A*, 128, 1
- Jones, T. & Whittet, D. 2015, *Interstellar polarization* (Cambridge University Press), 147–161
- Karalidi, T., Stam, D. M., & Hovenier, J. W. 2012, *A&A*, 548, A90
- Kawata, Y. 1978, *Icarus*, 33, 217
- Kemp, J. C., Henson, G. D., Steiner, C. T., & Powell, E. R. 1987, *Nature*, 326, 270
- Kemp, J. C. & Wolstencroft, R. D. 1971, *Nature*, 232, 165
- Kemp, J. C. & Wolstencroft, R. D. 1972, *ApJ*, 176, L115
- Kiselev, N., Rosenbush, V., Levasseur-Regourd, A.-C., & Kolokolova, L. 2015, *Comets*, ed. L. Kolokolova, J. Hough, & A.-C. Levasseur-Regourd, 379
- Kostogryz, N. M., Yakobchuk, T. M., & Berdyugina, S. V. 2015, *The Astrophysical Journal*, 806, 97
- Lucas, P. W., Hough, J. H., Bailey, J. A., et al. 2009, *Monthly Notices of the Royal Astronomical Society*, 393, 229
- MacDermott, A. J., Barron, L. D., Brack, A., et al. 1996, *Planet. Space Sci.*, 44, 1441
- Martin, W. E., Hesse, E., Hough, J. H., & Gledhill, T. M. 2016, *J. Quant. Spectr. Rad. Transf.*, 170, 131

- McLean, W., Stam, D. M., Bagnulo, S., et al. 2017, *A&A*, 601, A142
- Meierhenrich, U. J., Thiemann, W. H.-P., Barbier, B., et al. 2002, *Origins of Life and Evolution of the Biosphere*, 32, 181
- Nagdimunov, L., Kolokolova, L., & Sparks, W. 2013, *Earth, Planets, and Space*, 65, 1167
- Patty, C. H. L., Visser, L. J. J., Ariese, F., et al. 2017, *J. Quant. Spectr. Rad. Transf.*, 189, 303
- Rossi, L. & Stam, D. 2017, *Astronomy & Astrophysics*
- Schmid, H. M., Joos, F., & Tschan, D. 2006, *A&A*, 452, 657
- Seager, S., Whitney, B., & Sasselov, D. 2000, *The Astrophysical Journal*, 540, 504
- Sparks, W., Germer, T. A., MacKenty, J. W., & Snik, F. 2012, *Appl. Opt.*, 51, 5495
- Sparks, W., Hough, J. H., Germer, T. A., Robb, F., & Kolokolova, L. 2012, *Planet. Space Sci.*, 72, 111
- Sparks, W. B., Hough, J., Germer, T. A., et al. 2009, *Proceedings of the National Academy of Science*, 106, 7816
- Sparks, W. B., Hough, J. H., & Bergeron, L. E. 2005, *Astrobiology*, 5, 737
- Stam, D. M. 2008, *A&A*, 482, 989
- Stam, D. M., De Haan, J. F., Hovenier, J. W., & Stammes, P. 1999, *J. Geophys. Res.*, 104, 16843
- Stam, D. M., Hovenier, J. W., & Waters, L. B. F. M. 2004, *A&A*, 428, 663
- Swedlund, J. B., Kemp, J. C., & Wolstencroft, R. D. 1972, *ApJ*, 178, 257
- Tomasko, M. G. & Doose, L. R. 1984, *Icarus*, 58, 1
- Wolstencroft, R. D. 1976, *Icarus*, 29, 235
- Wolstencroft, R. D. & Kemp, J. C. 1972, *ApJ*, 177, L137

Appendix A: Comparison with Kawata (1978)

The spatially resolved signals computed in Section 3.1 can be compared with those in Figs. 11, 12, and 13 of Kawata (1978). The comparison is limited since Kawata (1978) used no Earth-like cloud particles. The phase angle is, however, 53° , which is close to our value of 60° . Kawata's cloud particles have the same effective radius and variance as our Venus-like cloud particles, but since he used different wavelengths from us, the refractive index is different (i.e. 1.46 at 340 nm, 1.433 at 700 nm, and 1.43 at 1000 nm). Kawata used three atmosphere models. Model 1 has one layer of mixed gas and cloud particles. The gas scattering optical thickness at 365 nm is 6, and the cloud optical thickness 128. Model 2 consists of a lower layer with only cloud particles and an upper layer of gas. Model 3 has a lower layer with mixed cloud particles and gas, and an upper layer of gas.

Kawata compares the signals of these model atmospheres at 380 nm where the gas has a large influence, and at 700 nm, where the gas has little influence. His results for his Model 1 at 700 nm (Fig. 11 in Kawata 1978) should be comparable to those of our atmosphere Models B (the gas optical thickness in our atmospheric layers is only 0.036) and D with Venus-like particles. Indeed, our results show similar characteristics to those of Kawata: in the absence of significant scattering by gas above the clouds, the neutral band crossing the disk from north to south is similar (although in our model, the band is shifted somewhat to the limb), as are the signs of P_c . We also find the increase of P_c towards to limb. Our Model D shows an additional neutral band close to the terminator that is absent in the results of Kawata. This difference is probably due to the slight differences in atmosphere models, refractive index, depolarization factor for the Rayleigh scattering, and/or phase angle.

The results of Kawata in case the contribution of gas above the clouds is significant (his Fig. 12) are also similar to ours, except that in our model atmospheres, the gas optical thickness is much smaller: the presence of gas removes the north-south neutral band, leaving mostly positive P_c across the northern hemisphere, with the highest values towards the limb. We do not find the slightly negative region north of the equator and towards the terminator on the northern hemisphere (and reversed on the southern hemisphere) that shows up in Kawata's Fig. 12. Indeed, we adapted our model atmosphere, the cloud particles' properties, and the phase angle to simulate Kawata's Fig. 12 as closely as possible, and while then the overall shape of P_c across our planetary disk is very similar to that in Fig. 12 of Kawata, our maximum values (at the limb) are only about 0.017% while those found by Kawata appear to be higher than 0.020%. We do find a slightly negatively polarized region on the northern hemisphere (and a slightly positively polarized region on the southern hemisphere) at approximately the same location as in Fig. 12 of Kawata, except with values that are a factor of ten smaller than those of Kawata. We also find small regions with inverse polarization near the poles that are absent in Fig. 12 of Kawata. The origin of these discrepancies is unknown, as not all details on Kawata's numerical computations are known to us, but they are extremely small, in particular in absolute sense, and leave us confident in our results.

Appendix B: Additional figures

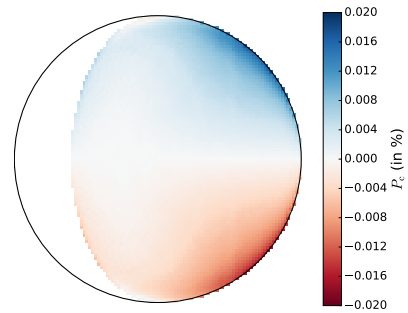


Fig. A.1: Degree of circular polarization P_c for $\alpha = 53^\circ$ and a model atmosphere as close as possible to that used in Fig. 12 by Kawata: the atmosphere consists of a single layer with $b_m = 0.51$ and cloud particles with $b_a = 128$. The cloud particles are described by a two-parameter gamma size distribution with $r_{\text{eff}} = 1.05 \mu\text{m}$ and $v_{\text{eff}} = 0.07$, with a refractive index equal to 1.458.

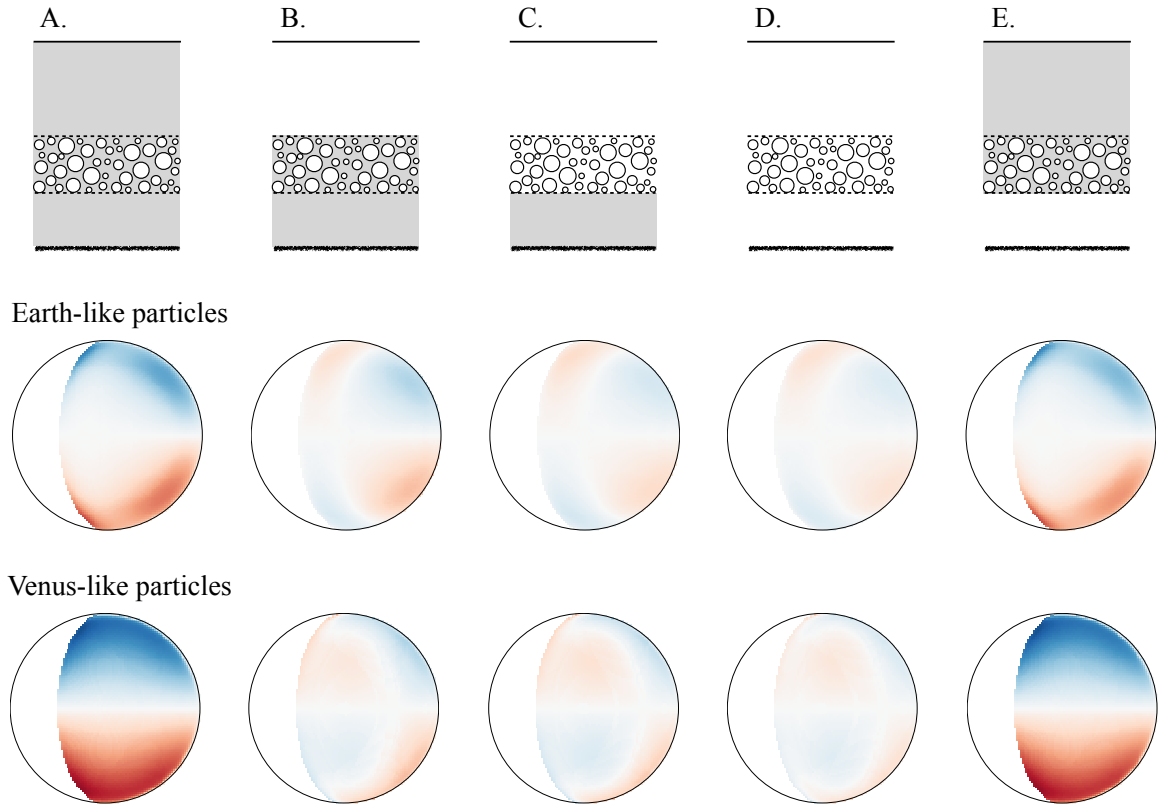
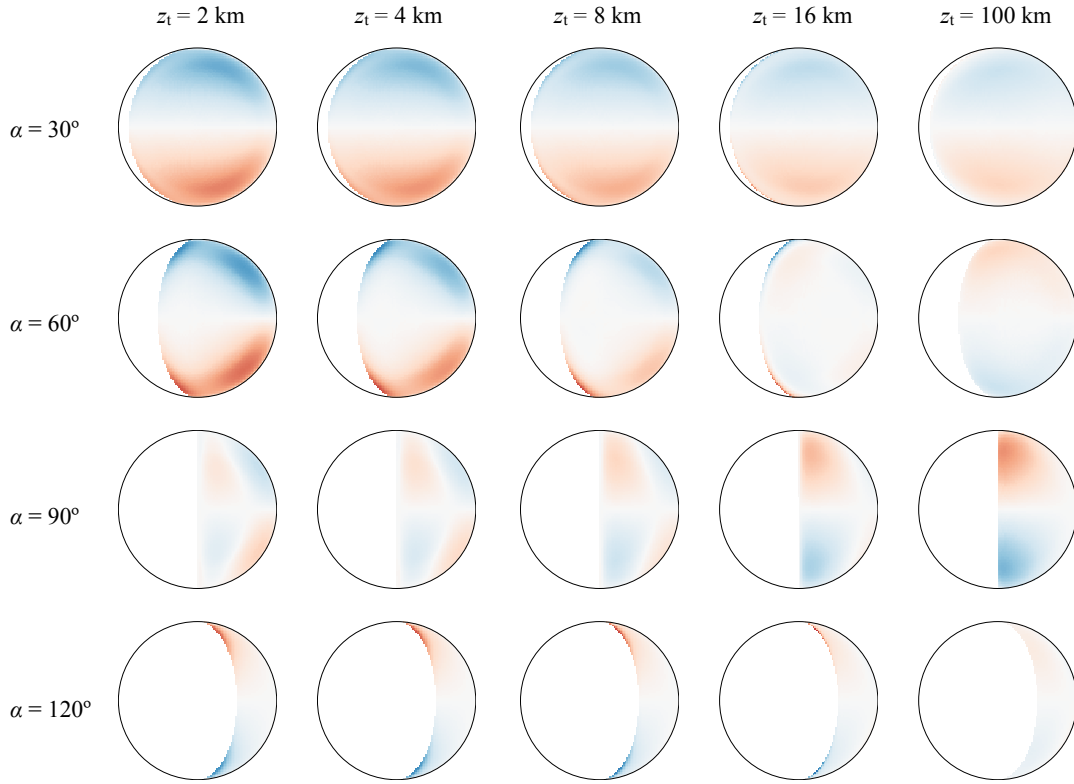


Fig. B.1: Similar to Fig. 3, except only for P_c and five different atmosphere models. The cloud top is at 4 km, the subdivision of the atmosphere above the cloud as in Fig. 1 is not shown. From left to right: A. gas in all atmospheric layers (cf. Fig. 3); B. only gas in the bottom and in the cloud layer; C. only gas in the bottom layer; D. no gas at all; E. no gas in the bottom layer.

Earth-like particles



Venus-like particles

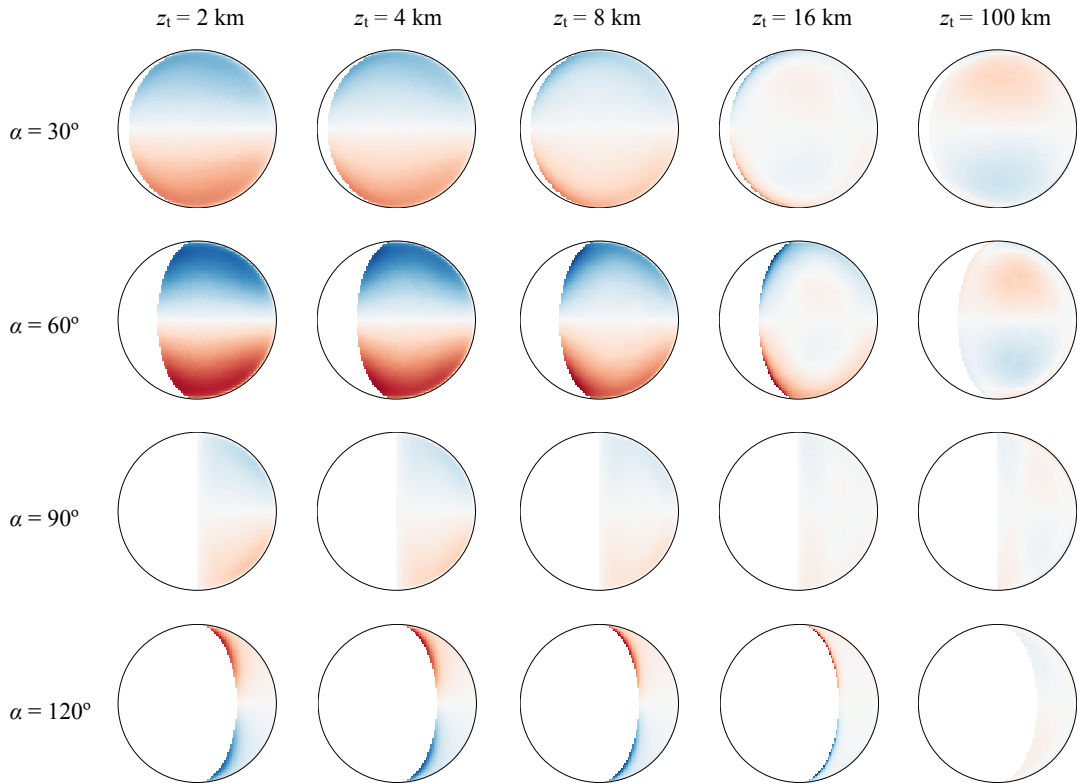
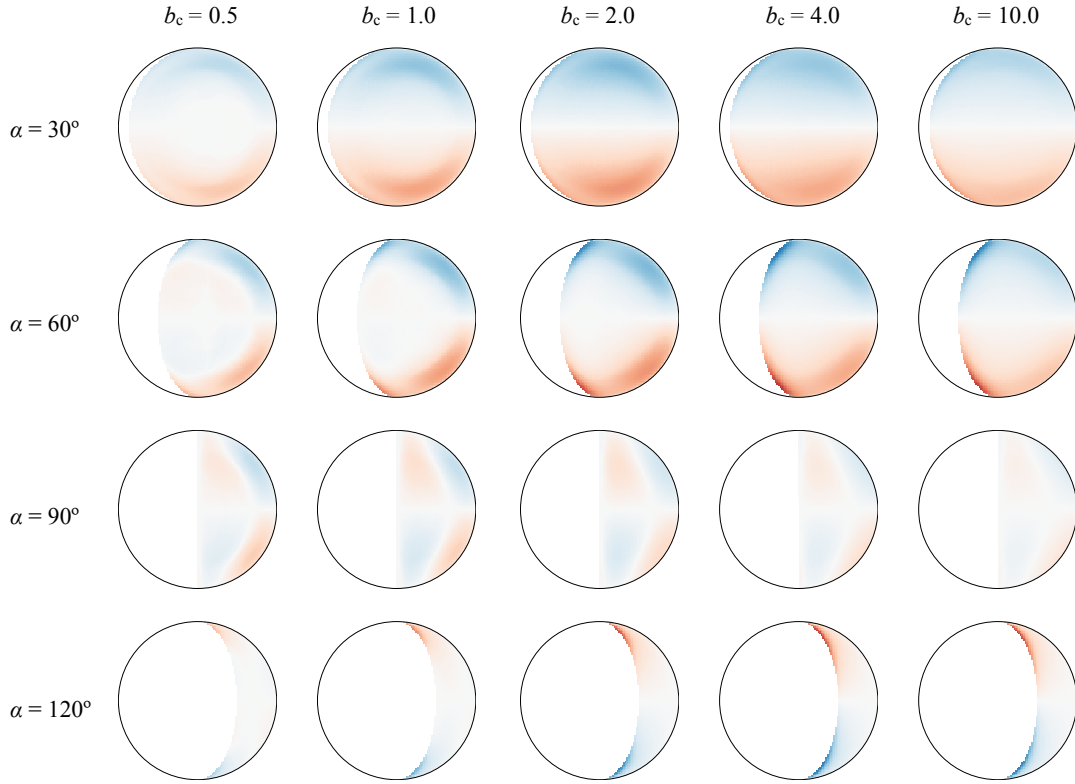


Fig. B.2: Degree of circular polarization P_c for α equal to 30° , 60° , 90° , and 120° . The standard model atmosphere has a $b_c = 2.0$ cloud consisting of Earth-like (top) or Venus-like (bottom) particles. The cloud top altitudes z_t are: 2 km (left columns), 4 km (cf. Fig. 3), 8 km, 16 km, and 100 km (right columns). The colour scale is the same as that in Fig. 3.

Earth-like particles



Venus-like particles

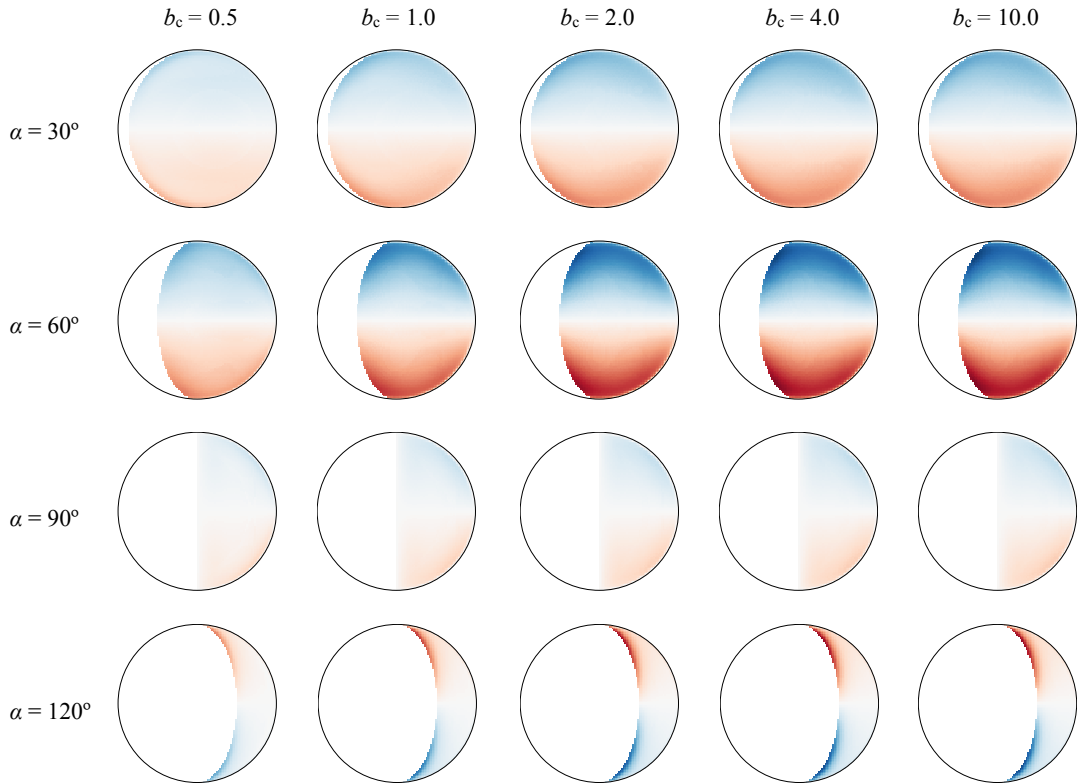


Fig. B.3: Degree of circular polarization P_c for α equal to 30° , 60° , 90° , and 120° . The standard model atmosphere has a cloud consisting of Earth-like (top) or Venus-like (bottom) particles, with the cloud top altitude $z_t = 4.0$ km, and the following cloud optical thicknesses b_c : 0.5 (left columns), 1.0, 2.0, 4.0, and 10.0 (right columns). The colour scale is the same as that in Fig. 3.